Storm time duskside equatorial current and its closure path

S. Dubyagin,[1] N. Ganushkina,[1,2] S. Apatenkov,[3] M. Kubyshkina,[3] S.-I. Ohtani,[4] H. Singer,[5] and M. Liemohn[2]

Received 25 January 2013; revised 9 August 2013; accepted 12 August 2013; published 12 September 2013.

[1] We study the closure path of the equatorial current which flows on the duskside in the inner magnetosphere during the moderate two-dip storm on 22 July 2009. This work was motivated by the result obtained in Tsyganenko and Sitnov (2007) that the prominent part of the duskside equatorial current might close through the dayside magnetopause during magnetic storms. Assuming the electric current conservation, we compared the value of the total downward region 2 current with the intensity of the equatorial current on the duskside to infer what part of the latter closes through the ionosphere. The estimates of the intensity of the equatorial current were based on the THEMIS and GOES magnetic field measurements in the vicinity of geosynchronous orbit. It was found that the duskside equatorial current intensifies simultaneously with Sym-H* decrease. However, unlike the conventional partial ring current, it occupies the region of the highly stretched magnetic configuration (magnetic field inclination $\sim 24°$ at $r = 5.4\ R_E$). At the same time, the magnetic field measurements onboard three DMSP satellites showed that the local time distribution of the storm time region 2 currents preserves the pattern typical for more quiet periods with upward (downward) current in the prenoon (afternoon) sector. The peak intensities of the downward region 2 current were recorded within 1 h from the Sym-H* minima in the vicinity of the dusk meridian. The peak values of the total downward region 2 current were found to be within 5–5.8 mA, while the intensity of the equatorial current at $R \approx 5.4$–$6.6 R_E$ was found to be 0.8–1.7 mA per 1 R_E. Keeping a current continuity, the radial extent of the partial ring current is estimated as 3.4–6 R_E. This indicates that most of the duskside current was diverted to the ionosphere during the main phase of this storm.

Citation: Dubyagin, S., N. Ganushkina, S. Apatenkov, M. Kubyshkina, S.-I. Ohtani, H. Singer, and M. Liemohn (2013), Storm time duskside equatorial current and its closure path, *J. Geophys. Res. Space Physics*, *118*, 5616–5625, doi:10.1002/jgra.50512.

1. Introduction

[2] The partial ring current (PRC) is one of the main storm time current systems, but it persists also during more quiet periods. It flows westward in the dusk-midnight sector of the inner magnetosphere and closes through the ionosphere via field-aligned currents (FAC). Originally, this system was proposed to explain the observed dusk-dawn asymmetry of the depression of the H component of the geomagnetic field at Earth's surface at middle and low latitudes during a main phase of magnetic storm [*Akasofu and Chapman*, 1964; *Cummings*, 1966; *Siscoe and Crooker*, 1974; *Crooker and Siscoe*, 1981]. However, it was later realized that the disturbance of the magnetic field in the inner magnetosphere exhibits mostly dayside-nightside asymmetry and weaker dusk-dawn asymmetry, in contrast with almost purely dusk-dawn asymmetry of the perturbed field at the ground [*Iijima et al.*, 1990; *Nakabe et al.*, 1997; *Terada et al.*, 1998; *Tsyganenko et al.*, 1999; *Le et al.*, 2004; *Ohtani et al.*, 2007]. Depending on the data used, the maximum of the equatorial part of the PRC was placed between the dusk and midnight meridian.

[3] The locations of the ionospheric closure of the PRC were mostly deduced indirectly from the statistical studies. On the basis of the average distribution of the large-scale Birkeland currents at low altitudes obtained by *Iijima and Potemra* [1976], the PRC closure was attributed to the region 2 current (equatorial part of large-scale FAC) [*Iijima and Potemra*, 1976; *Sato and Iijima*, 1979; *Tsyganenko*, 1993]. This is also in agrement with the average locations of the divergence and convergence of the equatorial current found in the vicinity of the dusk and dawn terminators [*Iijima et al.*, 1990; *Le et al.*, 2004]. However,

[1]Finnish Meteorological Institute, Helsinki, Finland.
[2]Department of Atmospheric, Oceanic and Space Sciences, University of Michigan, Ann Arbor, Michigan, USA.
[3]Earth Physics Department, St. Petersburg State University, St. Petersburg, Russia.
[4]Applied Physics Laboratory, Johns Hopkins University, Laurel, Maryland, USA.
[5]Space Weather Prediction Center, Boulder, Colorado, USA.

Corresponding author: S. V. Dubyagin, Finnish Meteorological Institute, Erik Palmenin aukio 1, Helsinki, FI-00101, Finland. (stepan.dubyagin@fmi.fi)

2169-9380/13/10.1002/jgra.50512

to our knowledge, there has been no direct evidence that region 2 current is connected to the partial ring current. In addition, *Wing et al.* [2010] showed that, statistically, the dayside region 2 current is linked with the different regions of the particle precipitations (inner magnetosphere, central plasma sheet, and plasma sheet boundary layer), not only the inner magnetosphere.

[4] A number of studies were conducted to locate the longitudinal sector of the PRC closure using both spaceborne and ground-based observations [*Iyemori*, 1990; *Nakano and Iyemori*, 2003, 2005]. The authors concluded that the downward current is located in the afternoon sector whereas the upward current is located in the midnight-postmidnight sector. However, these studies analyzed the combined effects from region 1 and region 2 FACs and additional assumptions were needed to separate the effect of region 2. Moreover, the ionospheric currents can contribute to the disturbance of the midlatitude ground magnetic field on the dayside.

[5] The storm time FAC were studied using the magnetic field measurements onboard of low-orbiting satellites [*Denig and Rich*, 1986; *Fujii et al.*, 1992; *Huang and Burke*, 2004; *Wang et al.*, 2006]. However, the afternoon sector was not covered by the observations and the PRC closure was not addressed in these studies. *Anderson et al.* [2005] studied the storm time large-scale Birkeland currents during 37 storms using the data from the Iridium constellation of satellites. The analysis revealed that the dusk FACs are shifted equatorward relative to dawn FACs. The authors concluded that this asymmetry is controlled by two independent factors, interplanetary magnetic field (IMF) B_y and an asymmetric inflation of the magnetosphere due to the partial ring current development.

[6] The generally accepted scenario of the PRC formation is that the plasma injected in the inner magnetosphere in the dusk-midnight sector drifts westward, creating the equatorial current which closes through the ionosphere at the leading and trailing edges of the plasma parcel [*Cahill*, 1966; *Bogott and Mozer*, 1973]. This scenario places the PRC in the region of the strong dipole-like magnetic configuration.

[7] The present study is motivated by the results of the recent empirical modeling of a storm time magnetic configuration [*Tsyganenko and Sitnov*, 2007; *Sitnov et al.*, 2008, 2010]. Unlike previous empirical models, the *Tsyganenko and Sitnov* [2007] model field is expanded in a series of basis functions of different scales which are able to reproduce the arbitrary radial and azimuthal variations. For every time, the model coefficients are found by fitting the model field to the observations during the periods with similar characteristics. In other words, the model represents the average configurations for given conditions. However, unlike the statistical 3-D magnetic field maps [*Terada et al.*, 1998; *Jorgensen et al.*, 2004; *Le et al.*, 2004], the model preserves the zero divergence of the magnetic field and electric current. The model shows that the currents in the inner magnetosphere can have a configuration significantly different from the conventional one during the main phase. The duskside current can occupy the broad area from $\sim$ 5 R_E to the magnetosphere's flank and close through the magnetopause on the dayside and the region 2 current in the postmidnight sector [*Sitnov et al.*, 2008].

[8] The principal goal of the present paper is to investigate the possible scenarios of the PRC closure. Assuming a conservation of current, we compare the current intensities in the duskside equatorial magnetosphere and total dawnward region 2 current on the dayside during the main phase of the moderate storm on 22 July 2009. The description of the storm is given in section 2. The estimation of the equatorial current from the Time History of Events and Macroscale Interactions during Substorms (THEMIS) [*Angelopoulos*, 2008] and GOES magnetic field observations are presented in section 3. The analysis of the dayside region 2 FAC intensities inferred from the DMSP magnetic field observations is presented in section 4. In section 5, we compare the equatorial current values and the values of the total region 2 current and discuss the possible errors. Our conclusions are presented in section 6.

2. Event Description and the Spacecraft Configurations

[9] We analyze the moderate magnetic storm on 22–24 July 2009 (minimum Sym-H = –93 nT). Figures1a–1c show the solar wind parameters, Figure 1d the Sym-H index, and Figures 1e–1f the configurations of the spacecraft orbits. The solar wind velocity (Figure 1a) started to grow from 300 km/s at ~0000 UT and reached ~ 500 km/s at ~1200 UT. The solar wind dynamic pressure (Figure 1b) exhibits a peak at ~0500 UT related to the peak of solar wind proton density (not shown). There were two periods when the z component of interplanetary magnetic field (IMF) dropped below –10 nT (Figure 1c) and the Sym-H index (blue curve in Figure 1d) exhibited two dips during these periods. To remove the influence of the dynamic pressure variation on the Sym-H index, we use the corrected Sym-H index which is denoted by Sym-H* = 0.8 Sym-H – 13 $\sqrt{P_{\mathrm{dyn}}}$ [*Tsyganenko*, 1996]. The Sym-H* index (black curve in Figure 1d) attained its minima at ~0520 UT and ~0905 UT. This storm has been analyzed in a number of studies and a more detailed description of the geomagnetic conditions can be found in *Ganushkina et al.* [2012].

[10] Figures 1e and 1f show the equatorial projection of the spacecraft orbits during two Sym-H* dip periods which are marked by red bars in Figure 1d. During the first Sym-H* dip (Figure 1e), GOES-11 was in the dusk sector whereas GOES-12 crossed midnight. The similar configuration was formed during the second intensification (Figure 1f): THEMIS D (P3) and E (P4) probes entered inside the geostationary orbit in the dusk sector, whereas GOES-11 crossed midnight. At the same time, GOES-12 was in the morning sector.

3. Analysis of Observations in the Equatorial Magnetosphere

[11] Figures 2a–2d show the observations of GOES-11, GOES-12, THEMIS-P3 (D), and P4 (E), respectively. We use the cylindrical solar magnetic (SM) coordinate system. The three components of the external (International Geomagnetic Reference Field has been subtracted) magnetic field B_r, B_φ, and B_z are shown in the bottom panel of each figure by blue, green, and red colors, respectively. The positive value of B_φ (azimuthal component) corresponds to the eastward direction of the magnetic field vector, B_z coincides with cartesian SM B_z, and B_r is the radial com-

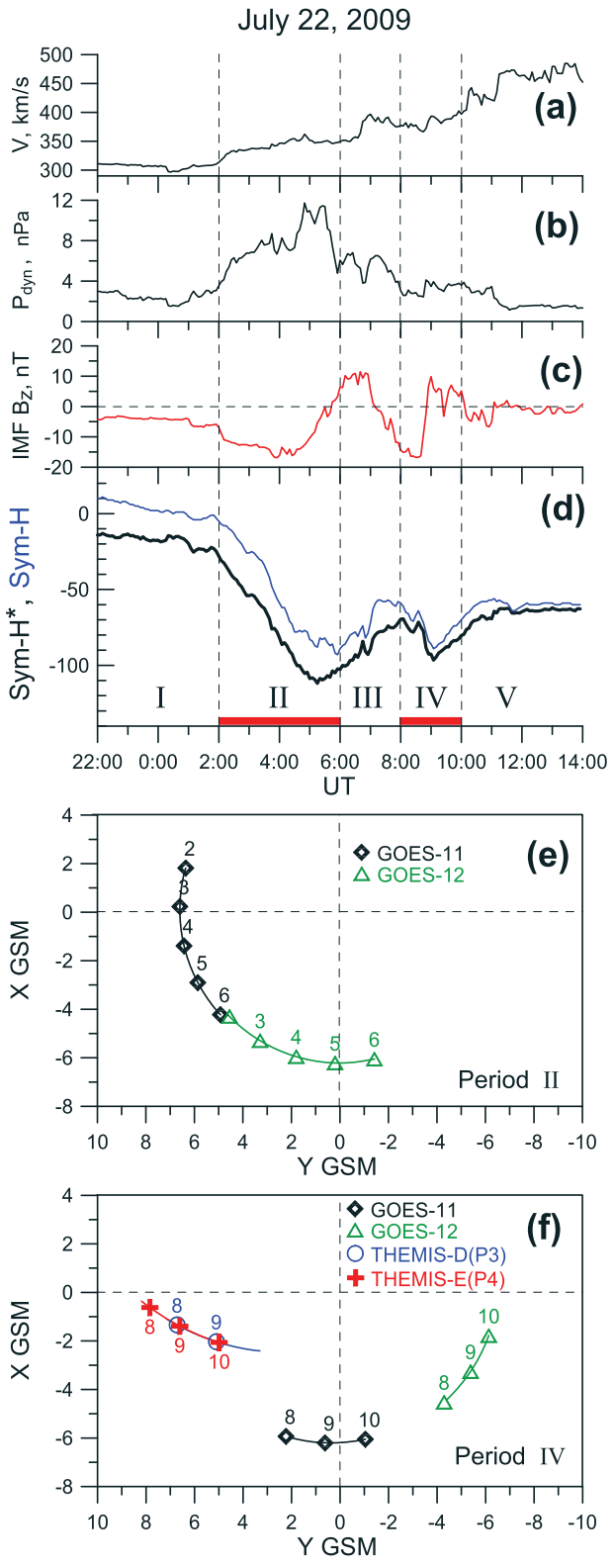

Figure 1. (a) Solar wind velocity, (b) solar wind dynamic pressure, (c) IMF B_z, (d) Sym-H index (blue) and solar wind pressure corrected Sym-H* (black). The vertical dashed lines demarcate five specific periods. (e–f) The spacecraft orbit configuration in the equatorial plane during two Sym-H* dips (periods II and IV). The labels at the symbols show the UT hours of 22 July 2009.

ponent. Three rows below the horizontal axis show UT, magnetic local time (MLT), and spacecraft position with respect to the neutral sheet (ΔZ_{NS}). The ΔZ_{NS} is defined as a distance along Z between a spacecraft and the model neutral sheet [*Tsyganenko and Fairfield*, 2004] for the solar wind parameters obtained from the OMNI database (http://omniweb.gsfs.nasa.gov/form/om_filt_min.html). In addition, the geocentric distance of spacecraft (R) is shown for THEMIS data (Figures 2c and 2d). The dashed vertical lines mark the times of the Sym-H* minima. The comparison of the observations with the *Tsyganenko and Sitnov* [2005] model field can be found in *Dubyagin et al.* [2013].

3.1. The First Sym-H* Minimum (04–06 UT)

[12] During the first Sym-H* minimum (~ 0520 UT), two geosynchronous spacecraft GOES-11 and GOES-12 were located at 20.1 and 0.2 MLT, respectively, approximately 1 R_E above the neutral sheet. The radial components (blue curves) of the external field at the dusk (GOES-11) and midnight (GOES-12) were very strong and negative ($\leq$ –100 nT). The B_z components (red curves) also were strong and negative ($\leq$ –70 nT) so that an extremely stretched configuration of magnetic field was formed over a wide MLT sector. The inclination of the full magnetic field vector at GOES-11 with respect to XY SM plane was ~ 11° (not shown). At the same time, the absolute value of B_φ was moderate (< 30 nT) and much smaller than $|B_r|$ and $|B_z|$, indicating that the current flowed in the azimuthal direction in the dusk-midnight MLT sector. Using Ampere's law, the azimuthal current integrated from $-Z_{SM}$ to $+Z_{SM}$, where Z_{SM} is the spacecraft position relative to the neutral sheet, can be estimated as $J = 2B_r/\mu_0$. Here, we neglect the term $\partial B_z/\partial r$ in comparison to $\partial B_r/\partial z$. Estimates of the possible error related to this simplification will be given at the end of this section. The estimates of J are plotted in the top panels in Figure 2 in mA/R_E units. As can be seen, the current values in the dusk sector (Figure 2a) and at midnight (Figure 2b) are of the same order during the Sym-H* minimum. Since the current sheet is considered to be thinnest in the premidnight sector during a storm main phase, the equality of the integrated current estimates in the dusk sector and at midnight could mean that these estimates represent the whole current or, equivalently, that both spacecraft were outside the current sheet.

3.2. The Second Sym-H* Minimum (08–10 UT)

[13] At 0905 UT, two THEMIS probes P3 (Figure 2c) and P4 (Figure 2d) were located ~ 0.1–0.5 R_E below the neutral sheet at MLT = 19.5 h, R = 5.4 R_E and MLT = 18.7 h, R = 6.7 R_E, respectively. Here, R is the geocentric distance. The signatures were basically the same as during the first Sym-H* dip; strong B_r (> 60 nT) and strong negative B_z (< –80 nT) with $B_\varphi \approx 0$ (Figures 2c and 2d). The inclination of the full magnetic field vector with respect to the XY SM plane at P3 and P4 probes was ~ 24° and ~ 6°, respectively (not shown). The maximum estimates of the integrated current give 0.6–0.8 MA/R_E. At the same time, GOES-11 was at midnight ~ 0.9 R_E above the neutral sheet and showed a comparable value of the integrated current (0.9 MA/R_E) just before the dipolarization occurred at ~ 0900 UT (Figure 2a).

[14] For this event, we can estimate the accuracy of current intensity evaluation. The relative error can be estimated

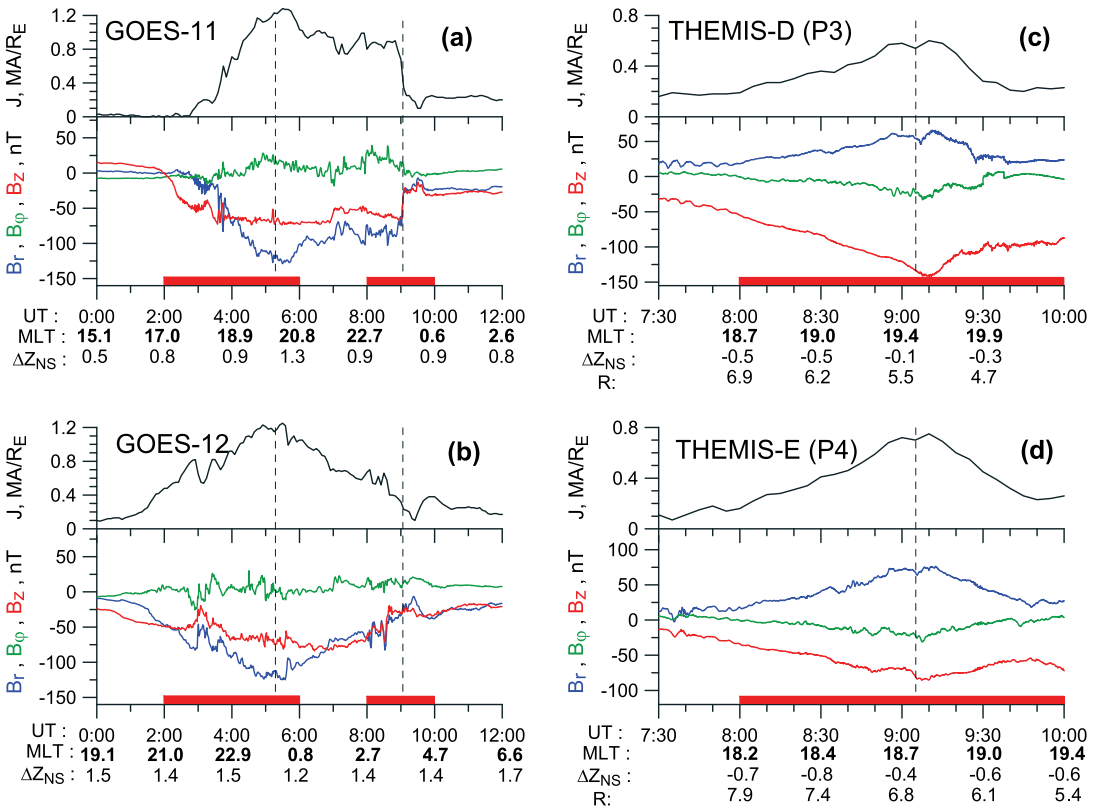

Figure 2. (a–d) The cylindrical SM components of the external magnetic field measured in the equatorial magnetosphere. The red bars mark the periods II and IV (see section 2).

as $\Delta J/J \approx (\partial B_z/\partial r)/(\partial B_r/\partial z)$. The $\partial B_r/\partial z$ can be roughly estimated as –68 nT/0.5 R_E (the radial component of the external field at P4 probe at 0905 UT divided by the estimated distance to the neutral sheet). The only way to estimate $\partial B_z/\partial r$ is to use the radial B_z gradient observed by two THEMIS probes around 0905 UT (see Figures 2c and 2d). It gives $\partial B_z/\partial r \approx$ (133–80 nT)/(6.7–5.4 R_E) = 41 nT/R_E. Finally, it gives us $\Delta J/J$ = 33%. The positive $\partial B_z/\partial r$ yields a westward current. Thus, this 33% should be added to the estimates of J obtained above. If we apply this correction to the integrated current estimate obtained during both Sym-H* minima, we get J =1.6–1.7 mA/R_E and J =0.8–1.0 mA/R_E for the first and second Sym-H* minima, respectively. These duskside equatorial current values will be compared with the dayside downward R2 FAC in section 5.

4. DMSP Magnetic Field Data Analysis

[15] In order to catch the downward field-aligned part of PRC with low-altitude satellite passes, we selected the DMSP F13, F16, and F17 satellite orbits on the dayside during the period 0000–1200 UT of 22 July 2009 (Figure 3). The analysis of the magnetic field observations and computation procedures were basically similar to those described by *Higuchi and Ohtani* [2000]. First, we converted the field measurements to solar magnetic (SM) coordinates (we use a spherical system: B_r, B_θ, and B_φ are radial, poloidal, and azimuthal components of the external field, respectively). Then we inspected the azimuthal component of the magnetic field. Large-scale variation of B_φ with the latitude mostly exhibited the signatures of the two-sheet FAC system: the increase (decrease) of B_φ with subsequent decrease (increase) to approximately the same level. Our purpose was to select the whole R2 FAC region, which is the most equatorial sheet of the field-aligned current, by definition. For this reason, we manually selected the equatorial interval of B_φ increase or decrease, ignoring local smaller-scale variations. The selection procedure is illustrated in Figure 4a. It shows an example of the DMSP magnetic field observations. The black, blue, and red curves corresponds to the B_φ, B_θ, and B_r components of external field in SM system, respectively. The satellite flew from the

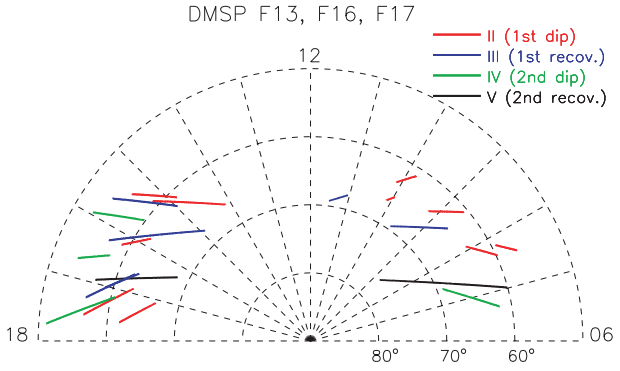

Figure 3. Polar plot of the DMSP orbit segments corresponding to R2 FAC. The colors correspond to the periods marked by Roman numbers in Figure 1a.

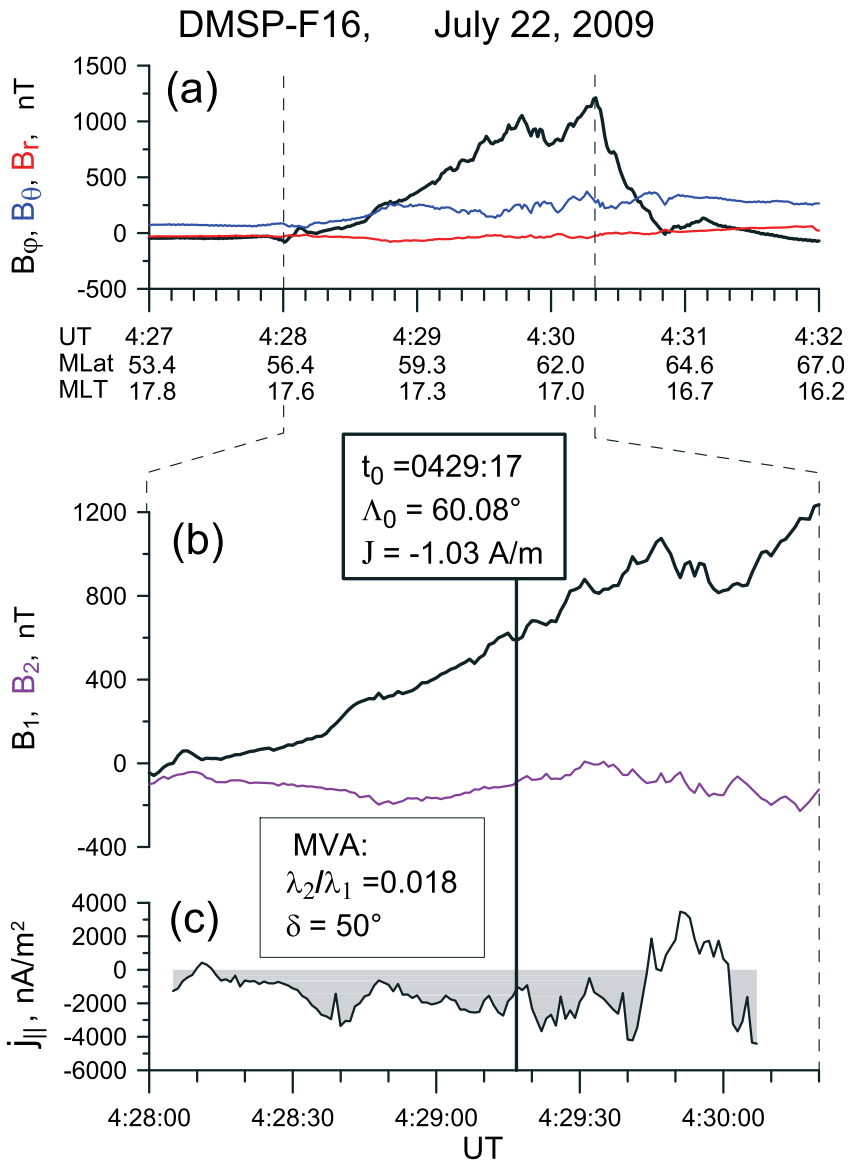

Figure 4. The example of DMSP magnetic field observations and minimum variance analysis (MVA) output. (a) Spherical components of observed magnetic field in SM coordinate system. (b) Horizontal magnetic field components corresponding to maximum and minimum variance directions. (c) Field-aligned current density estimated from the B_1 time series smoothed by a moving average.

equator to the pole at ~17 MLT. The gradual increase of the B_φ (approximately eastward) component corresponds to the downward current. We consider the interval 0428:00–0430:20 UT as a R2 current, ignoring the brief period of B_φ decrease at ~0429:55 UT. The B_φ decrease during 0430:20–0430:50 UT corresponds to R1 current.

[16] Figures 4b and 4c show the example of the FAC calculation. The minimum variance analysis (MVA) was applied to the horizontal components of the magnetic field measured in the equatorial part of large-scale FAC system (marked by dashed vertical lines in Figure 4a). The direction of the maximum variance was considered as a direction along the FAC sheet. Two parameters were used to control the quality of the determination of the FAC sheet orientation: the ratio of the minimum to the maximum eigenvalues (λ_2/λ_1) and the angle between the normal to the FAC sheet and the satellite velocity vector (δ). We only analyze the crossings with $\lambda_1/\lambda_2 < 0.2$ and $\delta < 60°$. The corresponding DMSP orbit segments are shown in Figure 3.

[17] For each point of the orbit, the local orthogonal coordinate system was defined. The $\mathbf{e_2}$ vector was defined as the minimum variance direction (if necessary, we multiplied $\mathbf{e_2}$ by –1 so that the angle between $\mathbf{e_2}$ and the satellite velocity was less than 90°). The $\mathbf{e_3}$ vector points toward local zenith and the $\mathbf{e_1}$ toward the maximum variance direction so that $\{\mathbf{e_1}, \mathbf{e_2}, \mathbf{e_3}\}$ form a right-handed system with corresponding magnetic field components: B_1, B_2, and B_3. Given the FAC sheet orientation, one can estimate the current density as

$$j_\parallel \approx -\frac{\partial B_1}{\mu_0 \partial x_2} \approx -\frac{\Delta B_1}{\mu_0 \Delta t V_{\mathrm{orb}} \cos(\delta)} \quad (1)$$

Table 1. Summary of the R2 FAC Sheet Crossings in the 06–12 MLT Sector

Satellite	t_0	δ	λ_2/λ_1	Λ_0	MLT (h)	J (A/m)	I^* (mA)
F-16	0258:48	53°	0.056	65.8	10.0	–0.28	–0.22
F-17	0350:58	49°	0.061	58.8	7.8	0.35	0.34
F-16	0442:16	59°	0.133	62.9	10.0	0.46	0.39
F-17	0532:56	52°	0.013	62.5	8.0	0.62	0.54
F-13	0556:30	45°	0.019	63.3	9.0	0.46	0.39
F-16	0622:36	54°	0.027	68.6	11.3	0.90	0.62
F-13	0738:28	43°	0.160	67.1	9.1	0.14	0.10
F-17	0858:14	38°	0.009	67.1	7.2	1.04	0.76
F-13	1103:43	41°	0.093	70.2	7.7	0.20	0.12

Here, V_{orb} is the orbital speed (7.4 km/s), δ is the angle between satellite velocity and $\mathbf{e_2}$, μ_0 is the vacuum permeability, and t is time.

[18] Figures 4b and 4c show the expanded view of the period selected for MVA. Figure 4b shows two components of the horizontal magnetic field disturbance in the MVA coordinate systems. Figure 4c shows the current density estimated using equation (1) (the B_1 time series was first smoothed by a moving average method with the 9 s window size). The negative and positive values correspond to the downward and upward currents, respectively.

[19] The integral of the current density across the current sheet can be estimated as

$$J \approx -\frac{1}{\mu_0}\Delta^{\text{tot}}B_1 \tag{2}$$

where $\Delta^{\text{tot}}B_1 = \pm(\max(B_1) - \min(B_1))$ is the total increment (decrement) of the B_1 component during the FAC sheet crossing, and the sign is determined according to whether B_1 increases or decreases from the equator to the pole. We also defined the center of current, the point of the orbit corresponding to the time t_0 determined as follows:

$$t_0 = \frac{\int j_{\parallel} t \mathrm{d}t}{\int j_{\parallel} \mathrm{d}t} \tag{3}$$

The equation is similar to that for center of gravity, but FAC density is used instead of mass density. The t_0 time marked in Figures 4b and 4c by the vertical solid line. Let Λ_0 denote the magnetic latitude of the center of current. Assuming that on the large scale, the current sheet is oriented along the constant magnetic latitude and does not change with MLT, we can estimate total R2 current for a given longitudinal extent ($\Delta\Phi$) as

$$I \approx J \cdot \Delta\Phi \cdot R \cdot \cos\Lambda_0 \tag{4}$$

where R is the geocentric distance of the satellite orbit estimated as $R = R_E + 850$ km. We define I^* as I computed for $\Delta\Phi = 1$ h MLT. That is, I^* is the R2 current flowing through the 1 h MLT sector. Below, we distinguish J, which is referred to as the current intensity, and I (or I^*), which are referred to as the total current.

[20] We divided our database of dayside R2 FAC crossings into two groups according to location with respect to noon. Tables 1 and 2 summarize the FAC sheet crossings in the 06–12 and 12–18 MLT sectors, respectively. We will refer to these sectors as prenoon and afternoon sectors. The fifth column of the tables shows Λ_0, the geomagnetic latitude of the center of current. As it can be seen, all the crossings occurred in the Northern Hemisphere.

[21] Figure 5 shows the large-scale FAC intensities, the IMF components, and the indices of geomagnetic activity. Grey triangles in Figure 5a correspond to the values of R2 current intensity in the prenoon sector and black circles corresponds to those in the afternoon sector. The labels at every symbol show the MLT of the crossing. It is seen that the polarity of R2 FAC during the storm time mostly correspond to average pattern found by *Iijima and Potemra* [1976], upward FAC in the prenoon and downward FAC in the afternoon. It means that if the PRC closes through the most equatorial part of the large-scale FAC system, it inflows in the afternoon sector. The peak intensity of the afternoon downward R2 FAC (–1.03 A/m) was recorded at ~ 0429 UT at the end of the main phase. The second peak was observed at ~0908 UT, and it coincided with the second Sym-H* minimum. Both peak intensities in the afternoon sector were observed at ~17 MLT. This may mean that afternoon R2 FAC intensity decreases from ~17 MLT toward the noon. The first peak of upward R2 FAC intensity in the prenoon sector was observed at ~ 0623 UT, 1 h later than first Sym-H* minimum. On the other hand, the

Table 2. Summary of the R2 FAC Sheet Crossings in the 12–18 MLT Sector

Sat.	t_0	δ	λ_2/λ_1	Λ_0	MLT (h)	J (A/m)	I^* (mA)
F-16	0247:11	52°	0.037	64.0	17.4	–0.60	–0.50
F-17	0338:19	59°	0.009	63.8	14.6	–0.44	–0.36
F-13	0401:25	51°	0.011	61.5	15.9	–0.49	–0.44
F-16	0429:17	50°	0.018	60.1	17.2	–1.03	–0.97
F-17	0519:37	47°	0.009	58.8	15.1	–0.60	–0.58
F-16	0612:42	37°	0.123	60.0	16.9	–0.70	–0.66
F-17	0702:43	28°	0.028	59.9	15.2	–0.18	–0.17
F-13	0727:58	43°	0.156	63.2	15.6	–0.35	–0.30
F-16	0756:10	50°	0.011	61.2	16.8	–0.52	–0.47
F-17	0843:50	45°	0.011	56.6	15.8	–0.64	–0.67
F-13	0907:45	31°	0.012	56.2	16.6	–0.79	–0.83
F-16	0936:57	28°	0.116	56.1	17.5	–0.36	–0.38
F-13	1050:09	22°	0.290	58.2	16.9	–0.11	–0.11

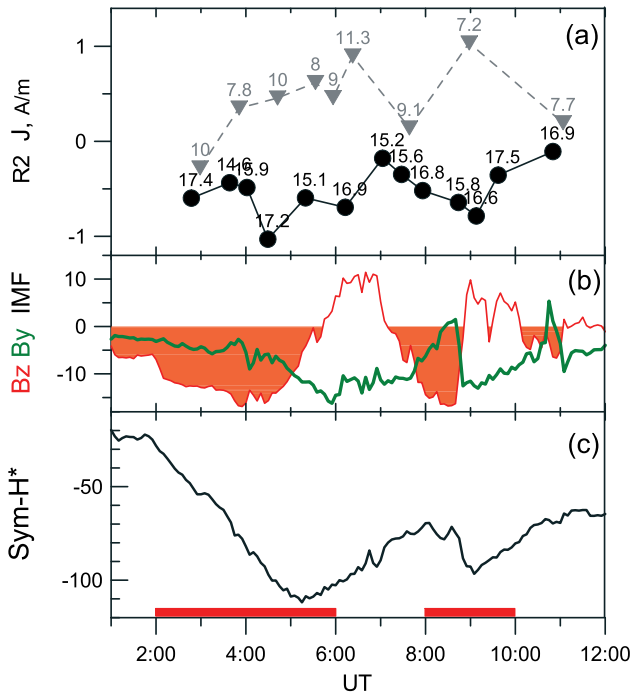

Figure 5. (a) The R2 FAC current intensity as deduced from DMSP magnetic field observations. Black circles (grey triangles) correspond to the flights in the afternoon (prenoon) MLT sector. The labels at the symbols show the MLT of the crossing. (b) IMF B_zB_y components. (c) Sym-H* index. The red horizontal bars mark the periods II and IV (see section 2).

second peak value of R2 FAC intensity in the prenoon sector was recorded close to the time of the second Sym-H* minimum. The R2 FAC intensities in both MLT sectors showed a minimum during the 0700–0740 interval when Sym-H* temporally recovered. The close relation of the downward R2 current intensity in the afternoon sector with the Sym-H* implies that this current is a closure of the partial ring current.

5. Comparison of Downward R2 FAC and Dusk Equatorial Current

[22] In section 4, we found that the maximum downward R2 current in the Northern Hemisphere during two Sym-H* minima was 0.97 and 0.83 mA per 1 h of MLT, respectively. However, to estimate the total downward R2 current on the dayside, we need to know how it varies with MLT. The peak values of the downward R2 current were observed at ~ 17 MLT. Figure 6 shows the absolute value of I^* in the afternoon sector as a function of MLT. We only plot the data corresponding to the periods of Sym-H* dip marked in Figure 1a by red bars and Roman numbers II and IV. These periods include also the early main phase and the Sym-H* recoveries when PRC is expected to be moderate. For that reason, one should focus on the top envelop of the data (dashed line) which shows a linear decrease from the dusk terminator to the midnoon. Assuming that the current linearly decreases from the peak values at 18 MLT (I^{*max}) to the zero value at the midnoon, we get the total downward R2 current in one hemisphere in 12–18 MLT sector $I^{R2} \approx 0.5 I^{*max} \cdot 6$ h. Assuming symmetry, two hemispheres give $I^{R2} \approx I^{*max} \cdot 6$ h. After substitution of $I^{*max} = 0.97$ mA and $I^{*max} = 0.83$ mA for two Sym-H* minima, we get $I^{R2} \approx 5.8$ mA and $I^{R2} \approx 5$ mA, respectively.

[23] Comparing the values of the R2 FAC and equatorial current, we consider three different scenarios of the duskside equatorial current closure: (1) through the ionosphere via R2 FAC, (2) through the dayside magnetopause, and (3) around the Earth (symmetric ring current). If we knew the value of the total duskside equatorial current (I^{dusk}), the difference $I^{dusk} - I^{R2}$ would give us an idea of what fraction of the duskside current closes through the magnetopause and around the Earth. Neglecting the symmetric ring current, we get an upper estimate of the current through the dayside magnetopause. However, only estimates of the duskside equatorial current intensity at one or two points are available. In section 3, we found that the equatorial current intensity in the vicinity of geosynchronous orbit on the duskside was $J^{dusk} \approx 1.6$–1.7 and $J^{dusk} \approx 0.8$–1.0 mA per 1 R_E of radial distance for the first and second Sym-H* minima, respectively. For the second Sym-H* minimum, the comparable values of the equatorial current intensity at the two THEMIS probes separated by ~1.3 R_E (section 3, Figures 2c and 2d) allow an estimate of the current flowing between these two probes as $J^{dusk} \times 1.3\ R_E \approx 1.0$–$1.3$ mA. However, it is only one-fourth of the downward R2 current. If one assumes that the z-integrated equatorial current is constant over some range of radial distance, the ratio I^{R2}/J^{dusk} shows that the size of the region of the equatorial current which is diverted to the ionosphere must be 3.4–6 R_E in radial extent to feed the observed downward R2 current. That is, nearly all of the duskside current must deviate to the ionosphere.

[24] The plot of the equatorial distribution of the current density in the model of *Tsyganenko and Sitnov* [2007] shows that the increased current density on the duskside during the

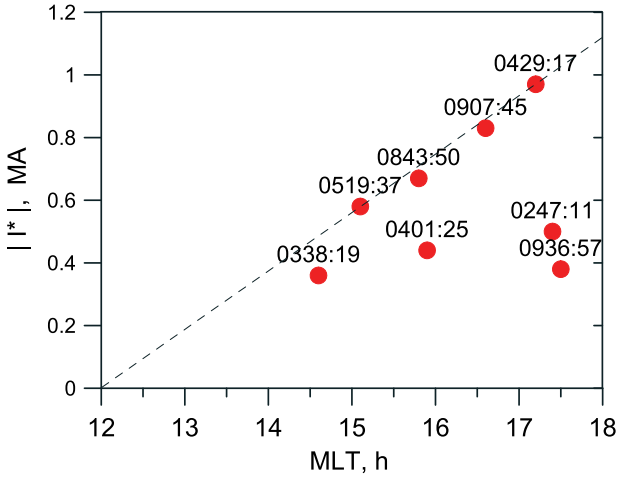

Figure 6. The absolute value of the R2 FAC current in the afternoon sector (circles) versus MLT for the periods II and IV (marked by red bar in Figure 1a). The dashed line depicts the position of the top envelope. The labels at the symbols show universal time.

main phase occupies at least 5 R_E in radial direction but peaks at $R \approx 5$–$6\ R_E$ and decreases with distance fast. On the other hand, the application of the same model to the moderate Corotating Interaction Region (CIR) driven storm [*Sitnov et al.*, 2010] showed that current density on the duskside can be increased over a larger region and show a more gradual decrease with distance just after the Sym-H minimum. However, only the inner part of the model current closes through the FAC whereas the remaining part closes through the dayside magnetopause.

[25] Our estimations rely on a number of assumptions. First, the estimations of the R2 FAC intensity were done using observations from DMSP in the Northern Hemisphere. In order to estimate the total R2 current flowing into both hemispheres, we multiply the obtained estimates by two, assuming the interhemispheric symmetry. However, many studies found seasonal dependance of the FAC due to higher ionospheric conductivity in the sunlit hemisphere [*Fujii et al.*, 1981, 1987; *Christiansen et al.*, 2002; *Haraguchi et al.*, 2004; *Ohtani et al.*, 2005; *Wang et al.*, 2005; *He et al.*, 2012]. It is commonly accepted that R1 intensities in the summer hemisphere is 1.5–3 times higher in comparison to the winter hemisphere. However, this conductivity influence is weaker for the R2 current [*Fujii and Iijima*, 1987; *Christiansen et al.*, 2002; *Haraguchi et al.*, 2004; *Ohtani et al.*, 2005]. Moreover, the dipole tilt angle attained its minimum ($\sim 10°$) at $\sim$ 0500 UT, the time of the first Sym-H* minimum. Thus, the conductivity influence was minimal during this period. If we accept that the R2 FAC is 1.5 times weaker in the Southern Hemisphere (lowest value of the ratio for R1 FAC), we get the total downward FAC density during two Sym-H* minima 4.1 mA and 4.8 mA, respectively.

[26] Second, temporal and spatial coverage of the DMSP passes on the dayside does not allow us to reconstruct the evolution of the R2 FAC MLT profile. On the basis of the DMSP observations during two periods of Sym-H* dip (6 h in total, Figure 6), we assumed that R2 current intensity decreases linearly from the dusk terminator to the midnoon. However, there were no observations available in the 12–14 MLT sector (see Figure 3). We can also estimate total downward R2 current summing the maximum values of $|I^*|$ for every hour of MLT where data are presented. In this case, we get the downward R2 FAC in one hemisphere 2.8 mA, and 5.6 mA for two hemispheres. We do not consider the configurations when R2 FAC intensity has a second maximum at midnoon.

[27] Third, the estimations of the duskside equatorial current are based on the assumption that the spacecraft is outside (above or below) or on the very edge of the current sheet. This assumption was validated by comparison of the z-integrated current estimated at the dusk and midnight which were found to be equal even though the midnight spacecraft was further from the neutral sheet than the dusk one. Moreover, our estimations are in agreement with the result of the statistical study by *Le et al.* [2004] who found current intensity of $\sim$ 150 μA/m at $\sim$ 19.5 MLT for the range –80 nT>Dst* > –100 nT (150 μA/m$\approx$ 1 mA/R_E). For the same range of Dst*, the authors found that total partial ring current integrated over the region $4\ R_E < R < 8\ R_E$; $-2\ R_E < Z < 2\ R_E$ is $\sim$ 2.6 mA. This value is two times smaller than our estimate of the downward R2 FAC.

6. Discussion

[28] We have studied the magnetic effect of the duskside equatorial current in the equatorial magnetosphere and above the ionosphere during the main phase of the moderate storm on 22 July 2009. The magnetic field observations in the equatorial magnetosphere revealed the existence of the sheet of westward current in 18–20 MLT sector at $R \approx 5.4$–$6.6\ R_E$. This current intensifies simultaneously with Sym-H* decrease. Unlike conventional PRC, this current occupies the region of the highly stretched magnetic configuration (the magnetic field inclination with respect to the XY SM plane was only 24° at $R = 5.4\ R_E$). At the same time, three DMSP satellites regularly crossed the dayside large-scale FAC system in the Northern Hemisphere. We used these data to reconstruct the evolution of the R2 current during the storm. It was found that the direction of the R2 FAC shows the standard pattern [*Iijima and Potemra*, 1976] with downward (upward) current on the duskside (dawnside; the sector 12–14 MLT was not covered). This finding implies that PRC closes through the afternoon part of the dayside ionosphere. The peak intensities of the downward R2 current were recorded within 1 h from the Sym-H* minima at 16–18 MLT. This finding is in agreement with results of *Liemohn et al.* [2001] which show that the PRC makes the main contribution to the Dst and Sym-H indices during the main phase. The locations of the recorded peak currents were close to the dusk terminator, and this is in agreement with the average location of the divergency of the equatorial current during disturbed conditions [*Iijima et al.*, 1990; *Le et al.*, 2004].

[29] Recent advanced empirical modeling [*Tsyganenko and Sitnov*, 2007; *Sitnov et al.*, 2008, 2010] has shown that a prominent part of the duskside current can close through the dayside magnetopause. In section 5, we compared the equatorial duskside current intensity at $\sim$ 18–20 MLT with the total downward R2 current in the 12–18 MLT sector. The peak values of the total downward R2 current on the dayside were found to be within 5–5.8 mA. At the same time, the intensity of the equatorial current at $R \approx 5.4$–$6.6\ R_E$ was found to be 0.8–1.7 mA per 1 R_E of the radial distance. If one assumes that the entire dayside R2 current closes through the equatorial region at 20 h MLT (where the estimations of the total equatorial current were made), the ratio of these values gives 3.4–6 R_E for the minimal PRC radial extent necessary to feed the observed R2 current. Saying "PRC radial extent," we mean the radial size of the region of the equatorial current diverted to the ionosphere. However, this estimate should not be understood literally. Various configurations are possible (e.g., outer parts of the equatorial current divert to the ionosphere, whereas the current in the vicinity of the neutral sheet continues to flow in the equatorial plane). This estimate just means that a significant fraction, perhaps most, of the duskside current was diverted to the ionosphere during the main phase of this storm. In such a configuration, it is questionable what current could close through the dayside magnetopause in this particular event. It should be noted that the equatorial current closure via dayside magnetopause is not equivalent to the convection outflow and the related mechanism of the ring current ions loss [*Takahashi et al.*, 1990; *Liemohn et al.*, 1999], which could persist independently of the current closure.

7. Summary

[30] Using the observations in the inner magnetosphere and at low altitudes, we studied behavior of the duskside equatorial current and R2 field-aligned current system during the two-dip storm on 22 July 2009. The following features have been found:

[31] 1. The equatorial current in 18–20 MLT sector at R = 5.4–6.6 R_E occupied the region of the highly stretched magnetic configuration.

[32] 2. The direction of the R2 field-aligned current on the dayside was the same as it was found for moderately disturbed conditions by *Iijima and Potemra* [1976]: the downward current in the noon-evening sector, upward current in the morning-noon sector, and the peak intensities of the downward current were recorded at 16.5–18 MLT.

[33] 3. Both duskside equatorial current and downward R2 field-aligned current intensified with Sym-H* decrease.

[34] 4. The comparison of the total downward R2 current to the z-integrated equatorial current on the duskside shows that a prominent part, probably most or even all, of the duskside current closes through the ionosphere during the main phase of the storm.

[35] The presented analysis is a case study and the results can not be generalized. However, this work shows how the current continuity can be used to study the current system configuration. This work also elicits the problems which should be solved in the future statistical studies. One of these problems is the limited information about the FAC distribution on the dayside. The Active Magnetosphere and Planetary Electrodynamics Response Experiment system (AMPERE, http://ampere.jhuapl.edu), which started to operate recently, provides the map of the strong FAC in both hemispheres at high temporal resolution. The more detailed statistical study of the current balance in the inner magnetosphere is needed.

[36] **Acknowledgments.** Work by S.D. was supported by the Academy of Finland. The authors thank the International Space Science Institute in Bern, Switzerland, for their support of an international team on "Resolving Current Systems in Geospace." Work by N.G. was partly supported by NASA, NSF, and Academy of Finland. Work by M.L. was supported by various NASA and NSF grants. Magnetospheric indices and solar wind parameters were obtained from the OMNI database provided by J.H. King, N. Papitashvilli at AdnetSystems, NASA GSFC. DMSP magnetometer data were provided by G. Wilson and the Air Force Research Laboratory, and we thank S. Wing for making it available for this study. GOES data were obtained via the CDAWeb. Thanks to K. H. Glassmeier, U. Auster, and W. Baumjohann for the use of FGM data provided under the lead of the Technical University of Braunschweig and with financial support through the German Ministry for Economy and Technology and the German Center for Aviation and Space (DLR) under contract 50 OC 0302.

[37] Robert Lysak thanks the reviewers for their assistance in evaluating this paper.

References

Akasofu, S.-I., and S. Chapman (1964), On the asymmetric development of magnetic storm fields in low and middle latitudes, *Planet, Space Sci.*, *12*, 607–626.

Anderson, B. J., S.-I. Ohtani, H. Korth, and A. Ukhorskiy (2005), Storm time dawn-dusk asymmetry of the large-scale Birkeland currents, *J. Geophys. Res.*, *110*, A12220, doi:10.1029/2005JA011246.

Angelopoulos, V. (2008), The THEMIS mission, *Space Sci. Rev.*, *141*, 5–34.

Bogott, F. H., and F. S. Mozer (1973), ATS-5 observations of energetic proton injection, *J. Geophys. Res.*, *78*(34), 8113-Ű8118, doi:10.1029/JA078i034p08113.

Cahill, L. J. Jr. (1966), Inflation of the inner magnetosphere during a magnetic storm, *J. Geophys. Res.*, *71*(19), 4505–4519, doi:10.1029/JZ071i019p04505.

Christiansen, F., V. O. Papitashvili, and T. Neubert (2002), Seasonal variations of high-latitude field-aligned currents inferred from Ørsted and Magsat observations, *J. Geophys. Res.*, *107*(A2), 1029, doi:10.1029/2001JA900104.

Crooker, N. U., and G. L. Siscoe (1981), Birkeland currents as the cause of the low-latitude asymmetric disturbance field, *J. Geophys. Res.*, *86*(A13), 11,201–11,210, doi:10.1029/JA086iA13p11201.

Cummings, W. D. (1966), Asymmetric ring currents and the low-latitude disturbance daily variation, *J. Geophys. Res.*, *71*(19), 4495–4503, doi:10.1029/JZ071i019p04495.

Denig, W. F., and F. J. Rich (1986), The ionosphere-magnetosphere structure during a geomagnetic storm based on measurements in the morning auroral zone, *J. Geophys. Res.*, *91*(A1), 165–182, doi:10.1029/JA091iA01p00165.

Dubyagin, S., N. Ganushkina, S. Apatenkov, M. Kubyshkina, H. Singer, and M. Liemohn (2013), Geometry of duskside equatorial current during magnetic storm main phase as deduced from magnetospheric and low-altitude observations, *Ann. Geophys.*, *31*, 395–408, doi:10.5194/angeo-31-395-2013.

Fujii, R., T. Iijima, T. A. Potemra, and M. Sugiura (1981), Seasonal dependence of large-scale Birkeland currents, *Geophys. Res. Lett.*, *8*(10), 1103–1106, doi:10.1029/GL008i010p01103.

Fujii, R., and T. Iijima (1987), Control of the ionospheric conductivities on large-scale Birkeland current intensities under geomagnetic quiet conditions, *J. Geophys. Res.*, *92*(A5), 4505–4513, doi:10.1029/JA092iA05p04505.

Fujii, R., H. Fukunishi, S. Kokubun, M. Sugiura, F. Tohyama, H. Hayakawa, K. Tsuruda, and T. Okada (1992), Field-aligned current signatures during the March 13–14, 1989, great magnetic storm, *J. Geophys. Res.*, *97*(A7), 10,703–10,715, doi:10.1029/92JA00171.

Ganushkina, N. Y., S. Dubyagin, M. Kubyshkina, M. Liemohn, and A. Runov (2012), Inner magnetosphere currents during the CIR/HSS storm on July 21–23, 2009, *J. Geophys. Res.*, *117*, A00L04, doi:10.1029/2011JA017393.

Haraguchi, K., H. Kawano, K. Yumoto, S. Ohtani, T. Higuchi, and G. Ueno (2004), Ionospheric conductivity dependence of dayside region-0, 1, and 2 field-aligned current systems: Statistical study with DMSP-F7, *Ann. Geophys.*, *22*, 2775–2783, doi:10.5194/angeo-22-2775-2004.

He, M., J. Vogt, H. Lühr, E. Sorbalo, A. Blagau, G. Le, and G. Lu (2012), A high-resolution model of field-aligned currents through empirical orthogonal functions analysis (MFACE), *Geophys. Res. Lett.*, *39*, L18105, doi:10.1029/2012GL053168.

Higuchi, T., and S. Ohtani (2000), Automatic identification of large-scale field-aligned current structures, *J. Geophys. Res.*, *105*(A11), 25,305–25,315, doi:10.1029/2000JA900073.

Huang, C. Y., and W. J. Burke (2004), Transient sheets of field-aligned current observed by DMSP during the main phase of a magnetic superstorm, *J. Geophys. Res.*, *109*, A06303, doi:10.1029/2003JA010067.

Iijima, T., and T. A. Potemra (1976), The amplitude distribution of field-aligned currents at northern high latitudes observed by Triad, *J. Geophys. Res.*, *81*(13), 2165–2174, doi:10.1029/JA081i013p02165.

Iijima, T., T. A. Potemra, and L. J. Zanetti (1990), Large-scale characteristics of magnetospheric equatorial currents, *J. Geophys. Res.*, *95*(A2), 991–999, doi:10.1029/JA095iA02p00991.

Iyemori, T. (1990), Storm-time magnetospheric currents inferred from mid-latitude geomagnetic field variations, *J. Geomag. Geoelectr.*, *42*, 1249–1265.

Jorgensen, A. M., H. E. Spence, W. J. Hughes, and H. J. Singer (2004), A statistical study of the global structure of the ring current, *J. Geophys. Res.*, *109*, A12204, doi:10.1029/2003JA010090.

Le, G., C. T. Russell, and K. Takahashi (2004), Morphology of the ring current derived from magnetic field observations, *Ann. Geophys.*, *22*, 1267–1295, doi:10.5194/angeo-22-1267-2004.

Liemohn, M. W., J. U. Kozyra, V. K. Jordanova, G. V. Khazanov, M. F. Thomsen, and T. E. Cayton (1999), Analysis of early phase ring current recovery mechanisms during geomagnetic storms, *Geophys. Res. Lett.*, *26*(18), 2845–2848, doi:10.1029/1999GL900611.

Liemohn, M. W., J. U. Kozyra, M. F. Thomsen, J. L. Roeder, G. Lu, J. E. Borovsky, and T. E. Cayton (2001), Dominant role of the asymmetric ring current in producing the stormtime Dst*, *J. Geophys. Res.*, *106*(A6), 10,883–10,904, doi:10.1029/2000JA000326.

Nakabe, S., T. Iyemori, M. Sugiura, and J. A. Slavin (1997), A statistical study of the magnetic field structure in the inner magnetosphere, *J. Geophys. Res.*, *102*(A8), 17,571–17,582, doi:10.1029/97JA01181.

Nakano, S., and T. Iyemori (2003), Local time distribution of net field-aligned currents derived from high-altitude satellite data, *J. Geophys. Res.*, *108*(A8), 1314, doi:10.1029/2002JA009519.

Nakano, S., and T. Iyemori (2005), Storm-time field-aligned currents on the nightside inferred from ground-based magnetic data at midlatitudes: Relationships with the interplanetary magnetic field and substorms, *J. Geophys. Res.*, *110*, A07216, doi:10.1029/2004JA010737.

Ohtani, S., G. Ueno, T. Higuchi, and H. Kawano (2005), Annual and semi-annual variations of the location and intensity of large-scale field-aligned currents, *J. Geophys. Res.*, *110*, A01216, doi:10.1029/2004JA010634.

Ohtani, S., Y. Ebihara, and H. J. Singer (2007), Storm-time magnetic configurations at geosynchronous orbit: Comparison between the main and recovery phases, *J. Geophys. Res.*, *112*, A05202, doi:10.1029/2006JA011959.

Sato, T., and T. Iijima (1979), Primary sources of large-scale Birkeland currents, *Space Sci. Rev.*, *24*, 347–366.

Siscoe, G. L., and N. U. Crooker (1974), On the partial ring current contribution to Dst, *J. Geophys. Res.*, *79*(7), 1110–1112, doi:10.1029/JA079i007p01110.

Sitnov, M. I., N. A. Tsyganenko, A. Y. Ukhorskiy, and P. C. Brandt (2008), Dynamical data-based modeling of the storm-time geomagnetic field with enhanced spatial resolution, *J. Geophys. Res.*, *113*, A07218, doi:10.1029/2007JA013003.

Sitnov, M. I., N. A. Tsyganenko, A. Y. Ukhorskiy, B. J. Anderson, H. Korth, A. T. Y. Lui, and P. C. Brandt (2010), Empirical modeling of a CIR-driven magnetic storm, *J. Geophys. Res.*, *115*, A07231, doi:10.1029/2009JA015169.

Takahashi, S., T. Iyemori, and M. Takeda (1990), A simulation of the storm-time ring current, *Planet. Space Sci.*, *38*, 1133–1141.

Terada, N., T. Iyemori, M. Nosé, T. Nagai, H. Matsumoto, and T. Goka (1998), Storm-time magnetic field variations observed by the ETS-VI satellite, *Earth Planets Space*, *50*, 853–864.

Tsyganenko, N. A. (1993), A global analytical representation of the magnetic field produced by the region 2 Birkeland currents and the partial ring current, *J. Geophys. Res.*, *98*(A4), 5677–5690, doi:10.1029/92JA02002.

Tsyganenko, N. A. (1996), Effects of the solar wind conditions on the global magnetospheric configuration as deduced from data-based field models, in: *Proceedings of the Third International Conference on Substorms (ICS-3), Versailles, France, 12–17 May 1996*, 181–18.

Tsyganenko, N. A., G. Le, C. T. Russell, and T. Iyemori (1999), A study of the inner magnetosphere based on data of Polar, *J. Geophys. Res.*, *104*(A5), 10,275–10,283, doi:10.1029/1998JA900160.

Tsyganenko, N. A., and D. H. Fairfield (2004), Global shape of the magnetotail current sheet as derived from Geotail and Polar data, *J. Geophys. Res.*, *109*, A03218, doi:10.1029/2003JA010062.

Tsyganenko, N. A., and M. I. Sitnov (2005), Modeling the dynamics of the inner magnetosphere during strong geomagnetic storms, *J. Geophys. Res.*, *110*, A03208, doi:10.1029/2004JA010798.

Tsyganenko, N. A., and M. I. Sitnov (2007), Magnetospheric configurations from a high-resolution data-based magnetic field model, *J. Geophys. Res.*, *112*, A06225, doi:10.1029/2007JA012260.

Wang, H., H. Lühr, and S. Y. Ma (2005), Solar zenith angle and merging electric field control of field-aligned currents: A statistical study of the Southern Hemisphere, *J. Geophys. Res.*, *110*, A03306, doi:10.1029/2004JA010530.

Wang, H., H. Lühr, S. Y. Ma, J. Weygand, R. M. Skoug, and F. Yin (2006), Field-aligned currents observed by CHAMP during the intense 2003 geomagnetic storm events, *Ann. Geophys.*, *24*, 311–324, doi:10.5194/angeo-24-311-2006.

Wing, S., S. Ohtani, P. T. Newell, T. Higuchi, G. Ueno, and J. M. Weygand (2010), Dayside field-aligned current source regions, *J. Geophys. Res.*, *115*, A12215, doi:10.1029/2010JA015837.